Journal of Applied Polymer Science

Hybrid multi-scale epoxy composites containing conventional glass microfibers and electrospun glass nanofibers with improved mechanical properties

Yong Zhao, Tao Xu, Xiaojing Ma, Min Xi, David R. Salem, Hao Fong

Composite and Nanocomposite Advanced Manufacturing (CNAM) Center, South Dakota School of Mines and Technology, 501 East Saint Joseph Street, Rapid City, South Dakota 57701

Correspondence to: D. R. Salem (E-mail: David.Salem@sdsmt.edu) and H. Fong (E-mail: Hao.Fong@sdsmt.edu)

ABSTRACT: A mechanically flexible mat consisting of structurally amorphous SiO_2 (glass) nanofibers was first prepared by electrospinning followed by pyrolysis under optimized conditions and procedures. Thereafter, two types of hybrid multi-scale epoxy composites were fabricated *via* the technique of vacuum assisted resin transfer molding. For the first type of composites, six layers of conventional glass microfiber (GF) fabrics were infused with the epoxy resin containing shortened electrospun glass nanofibers (S-EGNFs). For the second type of composites, five layers of electrospun glass nanofiber mats (EGNF-mats) were sandwiched between six layers of conventional GF fabrics followed by the infusion of neat epoxy resin. For comparison, the (conventional) epoxy composites with six layers of GF fabrics alone were also fabricated as the control sample. Incorporation of EGNFs (i.e., S-EGNFs and EGNF-mats) into GF/epoxy composites led to significant improvements in mechanical properties, while the EGNF-mats outperformed S-EGNFs in the reinforcement of resin-rich interlaminar regions. The composites reinforced with EGNF-mats exhibited the highest mechanical properties overall; specifically, the impact absorption energy, interlaminar shear strength, flexural strength, flexural modulus, and work of fracture were (1097.3 ± 48.5) J/m, (42.2 ± 1.4) MPa, (387.1 ± 9.9) MPa, (12.9 ± 1.3) GPa, and (30.6 ± 1.8) kJ/m^2, corresponding to increases of 34.6%, 104.8%, 65.4%, 33.0%, and 56.1% compared to the control sample. This study suggests that EGNFs (particularly flexible EGNF-mats) would be an innovative type of nanoscale reinforcement for the development of high-performance structural composites. © 2015 Wiley Periodicals, Inc. J. Appl. Polym. Sci. **2015**, *132*, 42731.

KEYWORDS: composites; electrospinning; thermosets

Received 23 April 2015; accepted 14 July 2015

DOI: 10.1002/app.42731

INTRODUCTION

Polymer composites reinforced with high-performance fibers (*e.g.*, carbon fibers and glass fibers) have been widely used as structural materials for aerospace structures, ground vehicles, and sports equipment. The major advantages of polymer composites include high specific strength and toughness, as well as excellent corrosion resistance and fatigue tolerance.[1,2] In general, composite laminates reinforced with fabrics of glass fibers (or carbon fibers) exhibit excellent in-plane properties; whereas out-of-plane properties (*e.g.*, interlaminar shear strength and delamination toughness) are substantially lower, being dominated by the properties of the resin matrices.[3,4] In the recent years, nanoscale reinforcements have attracted growing interests for the fabrication of composites; and numerous research endeavors have indicated that the out-of-plane properties of such composites, in which nanoscale reinforcements are dispersed uniformly in the resin matrices, are significantly higher.[5–13] Among various nanoscale reinforcements, graphite nanofibers, nylon-6 nanofibers, carbon nanofibers, single/multi-walled carbon nanotubes, exfoliated graphite nano-platelets, layered silicates, and silica/glass nanoparticles have been extensively investigated.[8,13–23]

The technique of electrospinning provides a straightforward approach for the convenient preparation of fibers with diameters typically being hundreds of nanometers (commonly known as electrospun nanofibers).[24] Morphologically uniform and structurally amorphous SiO_2 (glass) nanofibers can be readily prepared by electrospinning a spin dope containing tetraethyl orthosilicate (TEOS) (an alkoxide precursor for making SiO_2) followed by pyrolysis in air.[25,26] In our recently reported study,[27] the reinforcement of electrospun glass nanofibers (EGNFs) in epoxy resin was investigated; and the experimental

Additional Supporting Information may be found in the online version of this article.

results revealed that the tensile strength, Young's modulus, work of fracture, and impact strength of the nano-epoxy composite resins with 1 wt % EGNFs were improved by 40, 201, 67, and 363%, respectively (compared to the neat epoxy resin). We also reported that, when the shortened EGNFs were used to partially replace conventional dental glass filler (i.e., a glass powder with particle sizes ranging from tens of nanometers to micrometers), the flexural strength, elastic modulus, and work of fracture of the resulting dental composites were substantially improved.[28] Nevertheless, the EGNFs (prepared in the form of overlaid nanofibrous mat) in the above studies were fragile and/or easy to break, suggesting the amount of structural defects in those EGNFs might be high. Hence, the mechanical properties (particularly tensile strength) of those EGNFs were probably low, which would have a detrimental effect on their reinforcement of resin matrices in composites.[27–29]

In this study, adjustments and optimizations of spin dope properties and pyrolysis conditions/procedures resulted in EGNFs in the form of mechanically flexible mats. The improved resilience of these mats presumably reflects mechanical properties of the EGNFs that are much higher than those of the EGNFs reported previously. Subsequently, two types of hybrid multi-scale epoxy composites were fabricated by the method of vacuum assisted resin transfer molding (VARTM).[16,30–32] For the first type of composites, six layers of conventional glass microfiber (GF) fabrics were infused with the nano-epoxy resin containing shortened flexible EGNFs. For the second type of composites, five layers of flexible EGNF mats were sandwiched between six layers of conventional GF fabrics followed by the infusion of neat epoxy resin. For comparison, the (conventional) composites with six layers of GF fabrics alone were also fabricated as the control sample. Thereafter, the mechanical properties (including the impact adsorption energy, interlaminar shear strength, and flexural properties) of the fabricated composites were evaluated, and their fracture surfaces were examined. Based upon the results obtained, possible reinforcement mechanisms are discussed.

EXPERIMENTAL

Materials

The epoxy resin, SC-15A, and the associated hardener, SC-15B, were supplied by Applied Poleramic. (Benicia, CA). The plain-woven fabric of conventional GFs (GFs, S-glass, 6 oz/yd^2) was purchased from Fisher Scientific (Pittsburgh, PA). TEOS (98%), polyvinyl pyrrolidone (PVP, Mw = 1,300,000), ethanol (EtOH, 99.5%), *N,N*-dimethyl formamide (DMF, 99%), dimethylsulfoxide (DMSO), and concentrated hydrochloric acid (~6*M* HCl in H_2O) were purchased from Sigma Aldrich.

Preparation of Flexible Electrospun Glass Nanofiber Mats

The flexible glass nanofiber mats were prepared by electrospinning of TEOS and PVP precursor nanofibers followed by pyrolysis in air, and the electrospinning parameters/conditions were determined upon optimization of previously reported research.[25] Prior to electrospinning, 7.24 g TEOS was mixed with 2.90 g HCl aqueous solution (made of 25 mL H_2O and three drops of concentrated hydrochloric acid) and 1.55 g EtOH followed by stirring for 12 h; meantime, 4.9 g PVP was dissolved in a solvent mixture of 29.18 g DMF and 8.75 g DMSO. Thereafter, the solutions of TEOS and PVP were mixed together followed by stirring for 1 h. The percentages of PVP and TEOS in the resulting spin dope were 9.0 and 13.3 wt %, respectively. The spin dope was then loaded in a 30 mL BD Luer-Lok^{TM} tip plastic syringe having an 18 gauge 90° blunt-end steel needle. The electrospinning was performed at 15 kV by using an ES30P high voltage supply (Gamma High Voltage Research, Inc.), and the feed rate was set at 1.0 mL/h by using a KDS 200 syringe pump (KD Scientific). The precursor nanofibers were collected on the electrically grounded aluminum foil that covered a laboratory-produced roller with diameter of 25 cm. The distance between the aluminum foil and the tip of needle was set at 25 cm. Subsequently, the electrospun precursor nanofiber mat was carefully separated from the aluminum foil, sandwiched between two ceramic plates, and placed in a Lindberg 54453 Heavy Duty Tube Furnace. The mechanically flexible electrospun glass nanofiber mats (denoted hereafter as EGNF-mats) were acquired upon pyrolysis of precursor nanofiber mats with the following optimal conditions/procedures: (1) increasing the temperature from 25°C to 180°C at 1°C/min; (2) holding the temperature at 180°C for 2 h; (3) increasing the temperature from 180°C to 325°C at 1°C/min; (4) holding the temperature at 325°C for 2 h; (5) increasing the temperature from 325°C to 800°C at 1°C/min; (6) holding the temperature at 800°C for 2 h; and (7) switching off the heat to cool the samples to room temperature. A constant flow of air was maintained through the furnace during the entire pyrolysis process, and the resulting EGNF-mats had a thickness of ~6 μm and a mass per unit area of ~2.5 g/m^2. To acquire the mechanically flexible mat, the pyrolysis profile has been optimized with three key factors as compared with that reported in previous work:[25] (1) since the boiling point of TEOS is ~169°C, the pyrolysis temperature was held at 180°C for 2 h to ensure the evaporation of residuals (i.e., the desorption of physically adsorbed water, alcohol, and other solvents), the phase transformation of TEOS from liquid to gas, and the condensation reaction that convert TEOS molecules into a mineral-like solid *via* the formation of Si—O—Si linkages; (2) in the temperature range from 300 to 400°C, a significant weight loss would occur in TEOS xerogels caused by the removal of organics (principally weight loss), polymerization, and shrinkage (in this temperature region, shrinkage is the structural relaxation process and proportional to weight loss);[33] therefore, the pyrolysis temperature was held at 325°C for 2 h; and (3) the precursor nanofibers could be converted into amorphous SiO_2 nanofibers between 600 and 1,000°C,[25] thus the final pyrolysis temperature was held at 800°C for 2 h consequently.

Preparation of Shortened Electrospun Glass Nanofibers

The prepared EGNF-mats were first cut into small pieces with both length and width of ~2 mm; subsequently, they were immersed in EtOH in order to be sonicated for 2 h with a Branson 2510 ultrasonic cleaner. Finally, the mixture was mechanically stirred at 800 rpm for 4 days with a Heidolph RZR 50 Heavy Duty Stirrer. After being dried at 80°C, the shortened EGNFs (denoted hereafter as S-EGNFs) with lengths of ~6 μm were obtained.

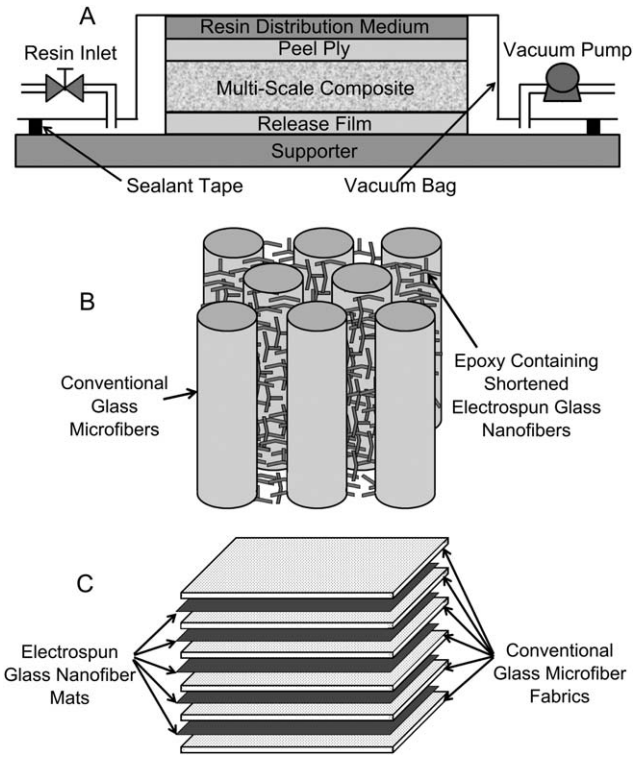

Figure 1. Schematics illustrating the VARTM process (A), the hybrid multi-scale composites fabricated from conventional GF fabrics and the nano-epoxy resin containing S-EGNFs (B), and the hybrid multi-scale composites fabricated from six layers of conventional GF fabrics and five layers of EGNF-mats (C).

Fabrication of Hybrid Multi-Scale Epoxy Composites

As shown schematically in Figure 1(A), the VARTM technique was adopted to fabricate the hybrid multi-scale epoxy composites; the epoxy resin was infused from the out-of-plane direction, and a vacuum of 27 mm Hg was applied during the infusion and the initial curing of epoxy resin. Two types of hybrid multi-scale epoxy composites were fabricated in this study. For the first type of composites, as depicted in Figure 1(B), the S-EGNFs were first dispersed into the SC-15A epoxy resin upon stirring at 600 rpm for 24 h; after that the SC-15B hardener was added into the nanofiber-containing SC-15A epoxy (with the mass ratio of 30/100) followed by hand-mixing for 5 min. Under the vacuum of 27 mm Hg, the prepared nano-epoxy resin (with 1.0 wt % S-EGNFs) was infused into the vacuum bag containing six layers of GF fabrics by the VARTM technique, and the initial curing was carried out at room temperature for 24 h. For the second type of composites, as depicted in Figure 1(C), six layers of conventional GF fabrics and five layers of EGNF-mats (with the length and width of 15 and 10 cm, respectively) were used to fabricate the hybrid multi-scale composites, and the mass ratio of six GF fabrics *versus* five EGNF mats was ~100/1. The mixture of SC-15A epoxy resin and the SC-15B hardener (with the mass ratio of 100/30) was then infused into the bag under the vacuum of 27 mm Hg, after which the system underwent the initial curing at room temperature for 24 h. Note that the mass ratio of epoxy resin *versus* six conventional GF fabrics was ~1/1 in the resulting multi-scale composite; therefore, the mass ratio of epoxy resin *versus* EGNFs (i.e., S-EGNFs or EGNF-mats) would be ~100/1. For comparison, the (conventional) composites with six GF fabrics alone were also fabricated as the control sample. Finally, before being characterized and evaluated, the initially cured composites (i.e., two types of hybrid multi-scale composites and the control (conventional) composites) were further cured in an oven at 110°C for 5 h to ensure the formation of epoxy composites (Supporting Information Figure S1).

Characterization and Evaluation

A Zeiss Supra 40 VP field-emission scanning electron microscope (SEM) was employed to examine the morphologies of fibers as well as the fracture surfaces of composites. Prior to SEM examinations, specimens were sputter-coated with gold for 30 s to avoid charge accumulations. The evaluation of mechanical properties was conducted under ambient conditions at room temperature. The Izod impact test was carried out by using a Tinius Olsen impact tester (Impact 104) according to ASTM D256. The three-point bending test with a span distance of 25.4 mm was conducted at a strain rate of 0.01 min^{-1} on a QTEST^{TM}/10 mechanical testing machine according to ASTM D790. The short-beam shear test was carried out on specimens with span-to-thickness ratio of 4, and a cross-head speed of 1 mm/min was maintained according to ASTM D2344. Five specimens of each composite were evaluated; subsequently, mean values and the associated standard deviations of the mechanical properties were calculated.

RESULTS AND DISCUSSION

Morphologies of GF Fabrics, EGNF-Mats, and S-EGNFs

The SEM images in Figure 2 were acquired from the conventional GF fabrics, EGNF-mats, and S-EGNFs, respectively. As shown in Figure 2(A), the GF fabrics were woven-fabrics made of conventional GF bundles with fiber diameters of ~10 μm. The SEM image in Figure 2(B) shows the representative morphology of EGNF-mats, which consisted of overlaid EGNFs with diameters of ~200 nm, and the nanofibers were continuous and relatively uniform without beads and/or beaded-nanofibers.[34] It is evident from the inset of Figure 2(B) that the EGNF-mat could be bent without formation of identifiable cracks and/or broken fibers, reflecting the mechanical flexibility of the prepared EGNF-mats (upon adopting the optimal pyrolysis profile). The prepared S-EGNFs [Figure 1(C)] had lengths of ~6 μm, diameters of ~200 nm, and thus the aspect ratios of ~30. It is noteworthy that all of the GF fabrics, EGNF-mats, and S-EGNFs were structurally amorphous, as evidenced by the acquired XRD curves (Supporting Information Figure S2), and the average fiber diameter of each sample was obtained through measuring 50 randomly selected fibers using the ImageJ software (histograms of fiber diameters for GF, EGNF, and S-EGNF are shown in Supporting Information Figure S3).

Mechanical Properties

Impact Absorption Energy. The Izod impact test of notched specimens was conducted to examine fracture behaviors of the fabricated composites; assessed by measuring the energy absorption after breaking the specimens at high strain rates. During the tests, the impact absorption energy results in deformation of the resin matrices, delamination of the composites, and breakage and/or pull-out of the fibers.[35] As shown in Figure 3(A), the

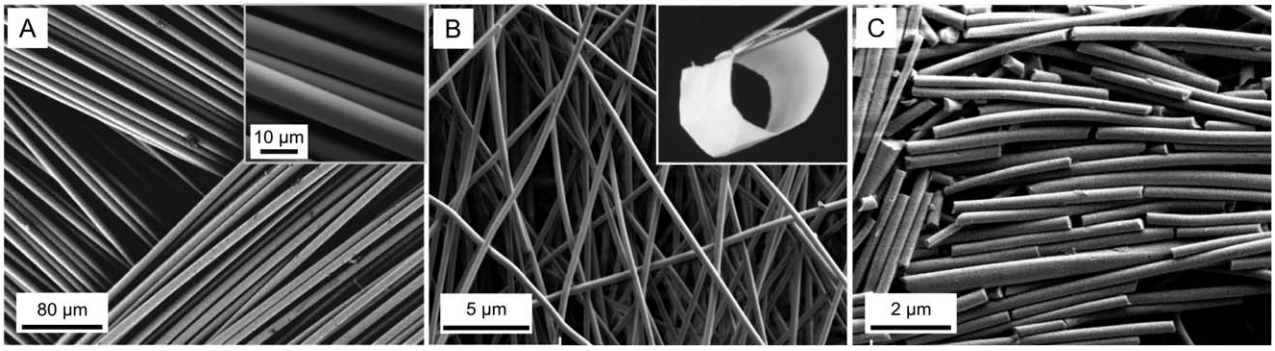

Figure 2. SEM images showing the representative morphologies of conventional GF fabrics (A), EGNF-mats (B), and S-EGNFs (C). Inset in 2A showing an SEM image of GF fabrics with higher magnifications. Photograph in 2B depicting the mechanical flexibility of EGNF-mats.

values of impact absorption energy were appreciably increased when 1.0 wt % EGNFs (i.e., S-EGNFs or EGNF-mats) were incorporated into the epoxy composite. The impact absorption energy of the control sample (i.e., GF/epoxy composites without EGNFs) was (815.0 ± 105.7) J/m; by comparison, the composites with EGNF-mats had an impact absorption energy of (1097.3 ± 48.5) J/m, while the composites with S-EGNFs exhibited the highest impact absorption energy of (1113.7 ± 138.5) J/m, representing an improvement of ~37% compared to the value of the control sample.

Interlaminar Shear Strength. It is noteworthy that, during the typical interlaminar short-beam shear and three-point bending tests of laminated composites, the shear stress is transferred from ply to ply through the resin matrix. Thus, delamination is one of the primary failure modes, while other failure modes (such as resin matrix cracking and fiber pull-out/debonding) may also contribute.[36,37] The evaluation of interlaminar shear strength for the fabricated composites was carried out by the short-beam shear test and calculated from the following Eq. (1):

$$\tau_s = 0.75 \frac{p_m}{b \times h} \quad (1)$$

where τ_s is the short-beam interlaminar shear strength (MPa), P_m is the maximum load during the test (N), b and h are the specimen width and thickness (mm), respectively.

Figure 4(A) shows the typical load-displacement curves acquired experimentally in the short-beam tests from the fabricated composites with and without EGNFs (i.e., S-EGNFs and EGNF-mats). It is evident that the incorporation of EGNFs into the composites substantially increased the flexural rigidity (stiffness) and maximum load at failure. As shown in Figure 3(B), the interlaminar shear strength of the control sample had the lowest value of (20.6 ± 1.7) MPa; the composites with S-EGNFs had a value of (40.2 ± 1.9) MPa, while the composites with EGNF-mats exhibited the highest interlaminar shear strength of (42.2 ± 1.4) MPa, representing an improvement of ~104.8% compared to the value of the control sample.

Flexural Strength. Figure 4(B) shows the typical load-displacement curves acquired experimentally in the three-point bending tests from the composites with and without EGNFs (i.e., S-EGNFs and EGNF-mats). Similar to the results in Figure 4(A), the composites with EGNFs had much higher stiffness and maximum load at failure. The flexural properties (i.e., strength, modulus, and work of fracture) of the tested composites are summarized in Table I. The acquired values of flexural strength and flexural modulus for the control sample were (234.1 ± 10.1) MPa and (9.7 ± 0.4) GPa, respectively; while the respective values for the composites with S-EGNFs were (323.7 ± 15.5) MPa and (11.9 ± 0.2) GPa, representing increases

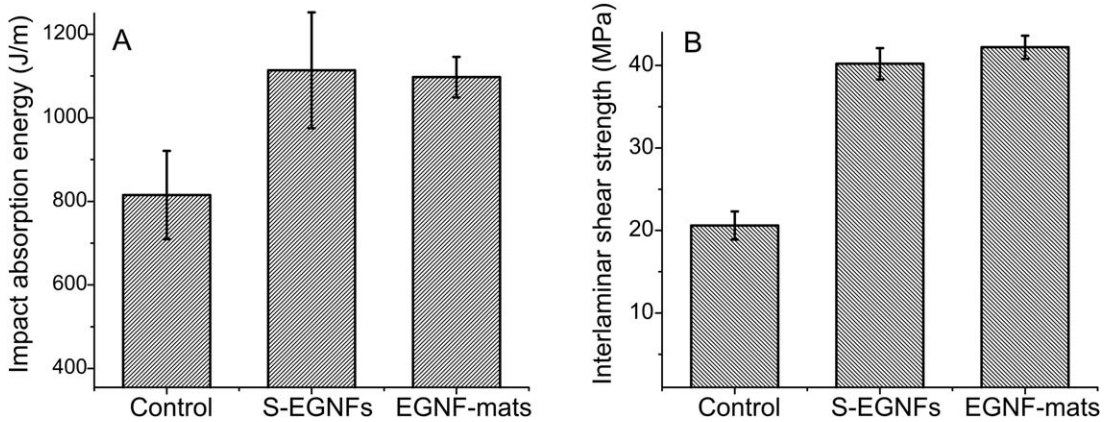

Figure 3. Impact absorption energy (A) and interlaminar shear strength (B) of three composites acquired from the Izod impact test and short-beam shear test. The control sample was the (conventional) GF/epoxy composites without EGNFs, and the hybrid multi-scale epoxy composites were incorporated with S-EGNFs and EGNFs-mats, respectively. Each datum showed the mean value of five measurements and the associated standard deviation.

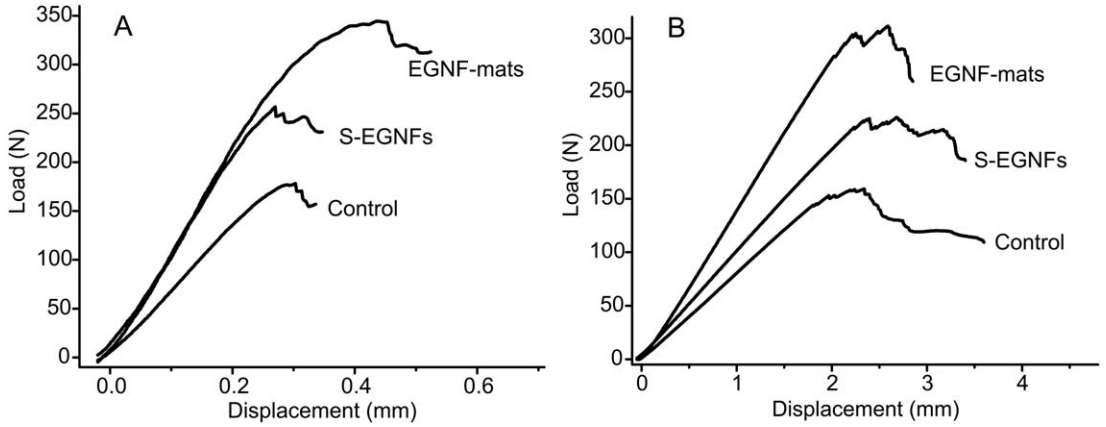

Figure 4. Typical load-displacement curves acquired from the short-beam shear test (A) and three-point bending test (B). The three composites included the control GF/epoxy composites (bottom curve), as well as the hybrid multi-scale GF/epoxy composites with S-EGNFs (middle curve) and EGNF-mats (top curve).

of 38.3% and 22.7%, respectively. The composites with EGNF-mats exhibited the highest flexural strength and flexural modulus of (387.1 ± 9.9) MPa and (12.9 ± 1.3) GPa, representing respective increases of 65.4% and 33.0% as compared to the values of the control sample.

Based on experimental load-displacement curves acquired from three-point bending tests, the work of fracture (WOF) of composites can be determined from the following Eq. (2):

$$\mathrm{WOF} = \frac{A}{bh} \tag{2}$$

where WOF is the work of fracture (kJ/m^2), b and h are the respective width and thickness of the specimen (m), A is the work done by the applied load to deflect/fracture the specimen (kJ), corresponding to the area under the load-displacement curve.

As shown in Table I, the WOF values increased after incorporation of EGNFs into the composites. The respective values of hybrid multi-scale composites with S-EGNFs and EGNFs-mats were (28.1 ± 1.1) and (30.6 ± 1.8) kJ/m^2, corresponding to increases of 43.3% and 56.1% relative to the control sample value of (19.6 ± 1.6) kJ/m^2. In general, in-plane mechanical properties of fiber-reinforced polymer composites are dominated by the mechanical properties and volume fraction of reinforcement fibers, while the incorporation of EGNFs into the composites (particularly in the interlaminar regions) is expected to be responsible for the observed increase in the flexural properties of the resulting GFs/EGNFs-epoxy composites. The EGNFs can strongly bond to the epoxy resin due to their large surface-to-volume ratio, resulting in improved interfacial bonding strength and, consequently, in higher flexural strength of the GFs/EGNFs-epoxy composite. Additionally, EGNFs could break and/or detach from epoxy resin matrix when the load is applied; this would dissipate the strain energy, impede the failure of the composite, and contribute to the higher value of WOF observed.

Table I. Flexural Properties of Three Composites Acquired from the Three-Point Bending Test

	Flexural properties		
Composites	Strength (MPa)	Modulus (GPa)	WOF (kJ/m^2)
Control	234.1 ± 10.1	9.7 ± 0.4	19.6 ± 1.6
S-EGNFs	323.7 ± 15.5	11.9 ± 0.2	28.1 ± 1.1
EGNF-mats	387.1 ± 9.9	12.9 ± 1.3	30.6 ± 1.8

The control sample was the (conventional) GF/epoxy composites without EGNFs, and the hybrid multi-scale epoxy composites were incorporated with S-EGNFs and EGNFs-mats, respectively. Each datum showed the mean value of five measurements and the associated standard deviation.

Fracture Surface and Reinforcement Mechanism

To understand the reinforcement mechanism of EGNFs (i.e., S-EGNFs and EGNF-mats) in hybrid multi-scale epoxy composites, the fracture surfaces of three-point bending specimens were examined by SEM. The images on the left of Figure 5 were acquired from the regions containing conventional GF fabrics, while the images on the right were acquired from the interlaminar regions. It is apparent from Figure 5(A) that in the control sample, the surfaces of conventional GFs were relatively smooth without residues of resin, and the matrix detached completely from the GFs due to weak interfacial bonding strength. In comparison, as shown in Figure 5(B,C), the conventional GFs in the hybrid multi-scale composites (with S-EGNFs or EGNF-mats) had much rougher surfaces, and were surrounded by and/or adhered to the epoxy resin, indicating that the interfacial bonding strength between the GFs and the epoxy resin were probably improved by the incorporation of S-EGNFs or EGNF-mats.

The fracture surfaces of failed composites may also provide valuable information about fracture mechanisms, as shown in Figure 5(D,E,F). From these figures, it is first necessary to note that the fracture surface of the SC-15 resin, with or without nanofiber reinforcement, reveals numerous, well-dispersed submicron specks. This is a characteristic feature of SC-15[38,39] and is believed to represent the phase-separated domains of the rubbery toughening component.[39] With regard to differences in fracture morphology arising from the presence of the S-EGNFs or EGNF-mats, it is evident that the control sample

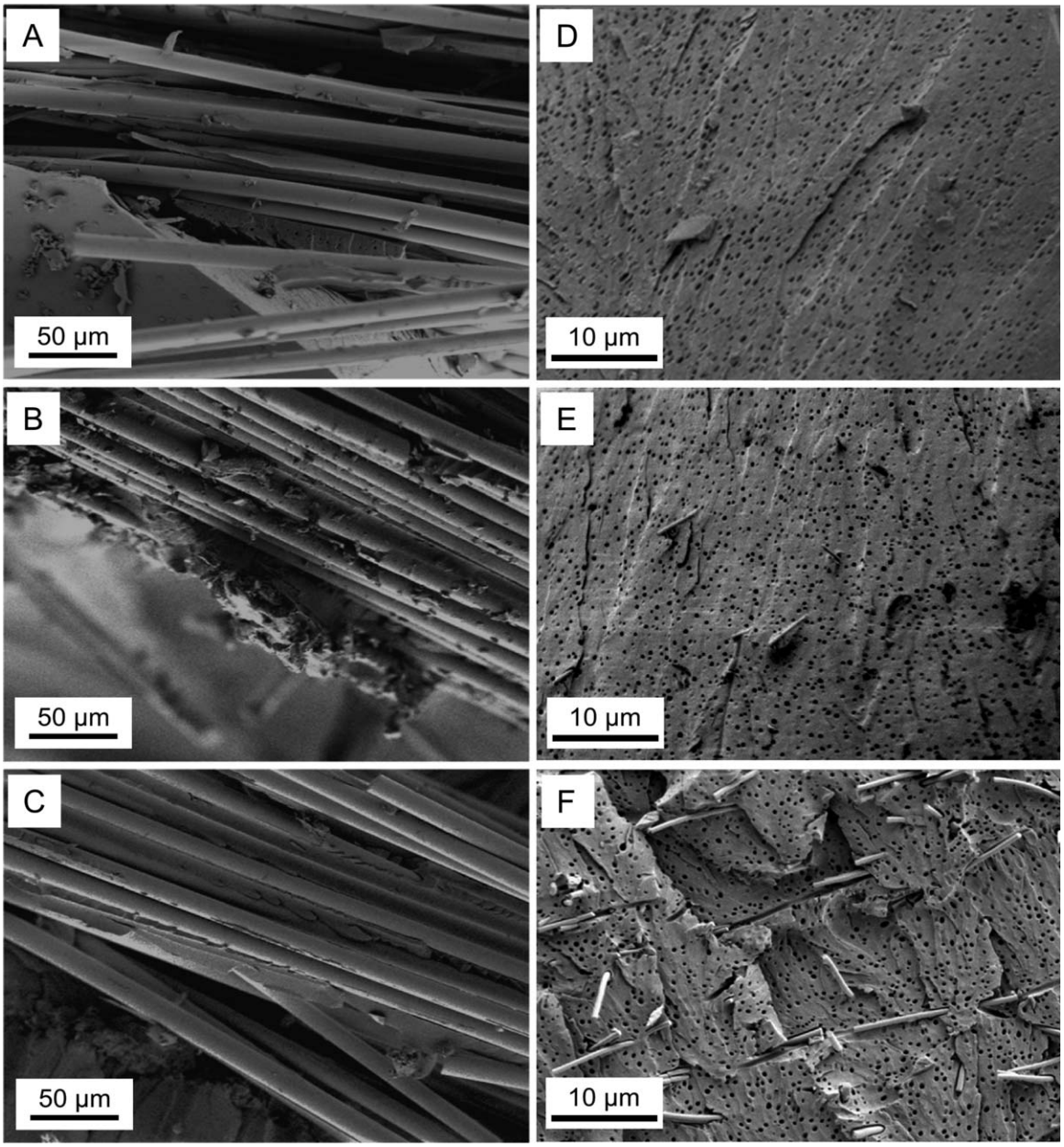

Figure 5. SEM images showing the representative fracture surfaces acquired from three-point bending specimens of the control GF/epoxy composites without EGNFs (A and D), GF/epoxy composites with 1.0 wt % S-EGNFs (B and E), and GF/epoxy composites with 1.0 wt % EGNFs-mats (C and F). The images on the left showing the regions containing conventional GF fabrics, while the images on the right showing the interlaminar regions.

[Figure 5(D)] shows a relatively smooth fracture surface with oriented fracture lines initiated from sites of crack growth. The lack of plastic deformation and the smooth fracture surface are in agreement with the materials having low toughness. In comparison, as shown in Figure 5(E,F), the hybrid multi-scale composites with S-EGNFs or EGNF-mats had rough features; and short, jagged, and multi-plane fracture lines can be observed on the fracture surfaces, especially in Figure 5(F). These observations may be attributed to the formation of a tougher interface between the epoxy matrix and EGNFs. Therefore, the main function of EGNFs in composites is probably to deflect the propagating cracks and force the crack growth to deviate from a given fracture plane. Additionally, the entanglement of EGNFs might mitigate the propagation of micro-cracks in the resin-rich interlaminar regions. Thus, if a micro-crack initiates in a region due to stress concentration, the entangled EGNFs remain intact across the crack plane and support the applied load, similar to the hooks and loops in Velcro.[40]

The fact that the composites with EGNF-mats [Figure 5(F)] had rougher fracture surfaces than the composites with S-EGNFs [Figure 5(E)] is consistent with the superiority of some of their mechanical properties (Figure 3 and Table I) and confirms that continuous EGNFs (i.e., EGNF-mats) tend to outperform short

EGNFs (i.e., S-EGNFs) in the reinforcement of resin-rich interlaminar regions in composites. It is well-known that the uniform dispersion of nanoscale reinforcements in resin matrix is essential for improving mechanical properties of the resulting hybrid multi-scale composites, and since the EGNF-mats were randomly overlaid/oriented, the nanofiber dispersion of EGNF-mats was arguably more uniform than that of S-EGNFs in the interlaminar regions. This may be one reason why the hybrid multi-scale composites with EGNF-mats exhibited the highest values of interlaminar shear strength and flexural properties. Another contributing factor may arise from the difference in load distribution in the two multi-scale hybrid composites: the continuous fiber network provided by the EGNF-mats in the interlaminar regions could more effectively redistribute the load than the discontinuous S-EGNFs, reducing the regions of stress concentration in the matrix, suppressing/mitigating matrix cracking, and leading to higher values of interlaminar shear strength and flexural strength.

CONCLUDING REMARKS

In this study, an overlaid mat consisting of structurally amorphous SiO_2 (glass) nanofibers was prepared by electrospinning followed by pyrolysis. Upon optimizing spin dope properties and pyrolysis procedures, the resulting EGNF mat was mechanically flexible, suggesting that the amount of structural defects in these EGNFs was low. Subsequently, hybrid multi-scale epoxy composites were fabricated by combining conventional GF fabrics with EGNFs (either continuous fiber EGNF mats or short EGNF fibers) and using the VARTM technique for resin infusion. The study revealed that the incorporation of EGNFs into GF/epoxy composites led to substantial improvements in out-of-plane mechanical properties and that the EGNF-mats outperformed short-fiber EGNFs (S-EGNFs). Specifically, for the EGNF-mats, the impact absorption energy, interlaminar shear strength, flexural strength, flexural modulus, and WOF were (1097.3 ± 48.5) J/m, (42.2 ± 1.4) MPa, (387.1 ± 9.9) MPa, (12.9 ± 1.3) GPa, and (30.6 ± 1.8) kJ/m^2, corresponding to increases of 34.6%, 104.8%, 65.4%, 33.0%, and 56.1% respectively, compared to the control sample of GF/epoxy composite (without EGNFs). This study suggests that EGNFs (particularly flexible EGNF-mats) could be an innovative type of nanoscale reinforcement for high-performance structural composites.

ACKNOWLEDGMENTS

This research was funded by the Composite and Nanocomposite Advanced Manufacturing (CNAM) Center, a research and development center supported by the Governor's Office of the state of South Dakota and by a consortium of corporations. All the work was performed at the South Dakota School of Mines and Technology.

REFERENCES

1. Mallick, P. K. Fiber-Reinforced Composites: Materials, Manufacturing, and Design. Marcel Dekker Inc.: New York, **1993**, p 1.
2. Luo, J. J.; Daniel, I. M. *Compos. Sci. Technol.* **2003**, *63*, 1607.
3. Zhu, J.; Imam, A.; Crane, R.; Lozano, K.; Khabashesku, V. N.; Barrera, E. V. *Compos. Sci. Technol.* **2007**, *67*, 1509.
4. Lubineau, G.; Rahaman, A. *Carbon* **2012**, *50*, 2377.
5. Bekyarova, E.; Thostenson, E. T.; Yu, A.; Kim, H.; Gao, J.; Tang, J.; Hahn, H. T.; Chou, T. W.; Itkis, M. E.; Haddon, R. C. *Langmuir* **2007**, *23*, 3970.
6. Kulkarni, M.; Carnahan, D.; Kulkarni, K.; Qian, D.; Abot, J. L. *Compos. Part. B: Eng.* **2010**, *41*, 414.
7. Zhamu, A.; Zhong, W. H.; Stone, J. J. *Compos. Sci. Technol.* **2006**, *66*, 2736.
8. Gaicia, E. J.; Wardle, B. L.; Hart, A. J. *Compos. Part. A: Appl. Sci. Manuf.* **2008**, *39*, 1065.
9. Zucchelli, A.; Focarete, M. L.; Gualandi, C.; Ramakrishna, S. *Polym. Adv. Technol.* **2011**, *22*, 339.
10. Jordan, J.; Jacob, K. I.; Tannenbaum, R.; Sharaf, M. A.; Jasiuk, I. *Mater. Sci. Eng. A* **2005**, *393*, 1.
11. Wang, B.; Zhou, X.; Yin, J.; Wang, L. *J. Appl. Polym. Sci.* **2013**, *128*, 990.
12. Wichmann, M. H. G.; Sumfleth, J.; Gojny, F. H.; Quaresimin, M.; Fiedler, B.; Schulte, K. *Eng. Fract. Mech.* **2006**, *73*, 2346.
13. Wu, X. F.; Rahman, A.; Zhou, Z.; Pelot, D. D.; Sinha-Ray, S.; Chen, B.; Payne, S.; Yarin, A. L. *J. Appl. Polym. Sci.* **2013**, *129*, 1383.
14. Park, J. K.; Do, I. H.; Askeland, P.; Lawrence, T. D. *Compos. Sci. Technol.* **2008**, *68*, 1734.
15. Tibbetts, G. G.; Lake, M. L.; Rice, B. P. *Compos. Sci. Technol.* **2007**, *67*, 1709.
16. Sadeghian, R.; Gangireddy, S.; Minaie, B.; Hsiao, K. T. *Compos. Part. A: Appl. Sci. Manuf.* **2006**, *37*, 1787.
17. Tsai, J. L.; Wu, M. D. *J. Compos. Mater.* **2008**, *42*, 553.
18. Kinloch, A. J.; Masania, K.; Taylor, A. C.; Sprenger, S.; Egan, D. *J. Mater. Sci.* **2008**, *43*, 1151.
19. Jiang, S.; Hou, H.; Greiner, A.; Agarwal, S. *ACS Appl. Mater. Interfaces* **2012**, *4*, 2597.
20. Jiang, S.; Greiner, A.; Agarwal, S. *Compos. Sci. Technol.* **2013**, *87*, 164.
21. Jiang, S.; Duan, G.; Hou, H.; Greiner, A.; Agarwal, S. *ACS Appl. Mater. Interfaces* **2012**, *4*, 4366.
22. Saha, A.; Jiang, C.; Marti, A. A. *Carbon* **2014**, *79*, 1.
23. Jiang, C.; Saha, A.; Xiang, C.; Young, C. C.; Tour, J. M.; Pasquali, M.; Marti, A. A. *ACS Nano* **2013**, *7*, 4503.
24. Dzenis, Y. *Science* **2004**, *304*, 1917.
25. Liu, Y.; Sagi, S.; Chandrasekar, R.; Hedin, N. E.; Fong, H. *J. Nanosci. Nanotechnol.* **2008**, *8*, 1528.
26. Wen, S.; Liu, L.; Zhang, L.; Chen, Q.; Zhang, L.; Fong, H. *Mater. Lett.* **2010**, *64*, 1517.
27. Chen, Q.; Zhang, L.; Yoon, M. K.; Wu, X. F.; Arefin, R. H.; Fong, H. *J. Appl. Polym. Sci.* **2012**, *124*, 444.
28. Gao, Y.; Sagi, S.; Zhang, L.; Liao, Y.; Cowles, D. M.; Sun, Y.; Fong, H. *J. Appl. Polym. Sci.* **2008**, *110*, 2063.
29. Zucchelli, A.; Focarete, M. L.; Gualandi, C.; Ramakrishna, S. *Polym. Adv. Technol.* **2011**, *22*, 339.

30. Kim, M.; Park, Y.; Okoli, O.; Zhang, C. *Compos. Sci. Technol.* **2009**, *69*, 335.

31. Zhou, Y.; Hosur, M.; Jeelani, S.; Mallick, P. K. *J. Mater. Sci.* **2012**, *47*, 5002.

32. Qiu, J.; Zhang, C.; Wang, B.; Liang, R. *Nanotechnology* **2007**, *18*, 1.

33. Rao, A. V.; Wagh, P. B.; Haranath, D.; Risbud, P. P.; Kumbhare, S. D. *Ceram. Int.* **1999**, *25*, 505.

34. Fong, H.; Chun, I.; Reneker, D. H. *Polymer* **1999**, *40*, 4585.

35. Schrauwen, B.; Bertens, P.; Peijs, T. *Polym. Polym. Compos.* **2002**, *10*, 259.

36. Li, J.; Sham, M. L.; Kim, J. K.; Marom, G. *Compos. Sci. Technol.* **2007**, *67*, 296.

37. Hibbs, M. F.; Tse, M. K.; Bradley, W. L. In Toughened Composites; Johnson, N. J. Ed.; ASTM STP, 937; American Society for Testing and Materials, **1987**, p 115.

38. Liao, Y. H.; Marietta-Tondin, O.; Liang, Z.; Zhang, C.; Wang, B. *Mater. Sci. Eng. A* **2004**, *385*, 175.

39. Wang, M. L.; McAninch, I. M.; La Scala, J. J. Materials Characterization of High-Temperature Epoxy Resins: SC-79 and SC-15/SC-79 blend. Army Research Laboratory Report, ARL-TR-5484, March **2011**.

40. Dzenis, Y. *Science* **2008**, *319*, 419.